View metadata, citation and similar papers at core.ac.uk
brought to you by CORE
provided by ethesis@nitr

Constant False Alarm Rate Target Detection in Synthetic Aperture Radar Imagery

Kumari Rosy Pradhan

Department of Electronics and Communication Engineering
National Institute of Technology Rourkela

Constant False Alarm Rate Target Detection in Synthetic Aperture Radar Imagery

Thesis submitted in partial fulfillment of the

requirements of the degree of

Master of Technology

in

Electronics and Communication Engineering
(*Specialization*: *Signal and Image Processing*)

by

Kumari Rosy Pradhan

(Roll Number: 214EC6394)

based on research carried out

under the supervision of

Prof. Lakshi Prosad Roy

May, 2016

Department of Electronics and Communication Engineering
National Institute of Technology Rourkela

Department of Electronics and Communication Engineering
National Institute of Technology Rourkela

Prof. Lakshi Prosad Roy
Professor

May 31, 2016

Supervisor's Certificate

This is to certify that the work presented in the thesis entitled *Constant False Alarm Rate Target Detection in Synthetic Aperture Radar Imagery submitted* by *Kumari Rosy Pradhan*, Roll Number 214EC6394, is a record of research carried out by her under my supervision and guidance in partial fulfillment of the requirements of the degree of *Master of Technology* in *Electronics and Communication Engineering*. Neither this thesis nor any part of it has been submitted earlier for any degree or diploma to any institute or university in India or abroad.

_____

Lakshi Prosad Roy
Principal Supervisor

dedicated to my family

Declaration of Originality

I, ***Kumari Rosy Pradhan***, Roll Number ***214EC6394*** hereby declare that this thesis entitled ***Constant False Alarm Rate Target Detection in Synthetic Aperture Radar Imagery*** presents my original work carried out as a M. Tech student of NIT Rourkela and, to the best of my knowledge, contains no material previously published or written by another person, nor any material presented by me for the award of any degree or diploma of NIT Rourkela or any other institution. Any contribution made to this research by others, with whom I have worked at NIT Rourkela or elsewhere, is explicitly acknowledged in the thesis. Works of other authors cited in this thesis have been duly acknowledged under the sections "Reference". I have also submitted my original research records to the scrutiny committee for evaluation of my thesis.

I am fully aware that in case of any non-compliance detected in future, the Senate of NIT Rourkela may withdraw the degree awarded to me on the basis of the present thesis.

May 27, 2016
NIT Rourkela

Kumari Rosy Pradhan
Roll Number:214EC6394

Acknowledgment

I would like to take opportunity to thank my supervisor **Prof. Lakshi Prosad Roy** for his guidance and active support during my thesis work. With his in-depth knowledge about the subject and great patience, he guided me through every hurdle of this project work. I am deeply grateful to him for teaching me both research and writing skills, which have been proved to be very beneficial for my career. It has been a great pleasure working under him and it was my good fortune to have such a person as my guide.

I am also very much indebted to **Prof. S. Meher**, **Prof. K.K. Mahapatra**, **Prof. S. K. Patra**, **Prof. S. Ari**, **Prof. M. Okade**, **Prof. A. K. Sahoo**, **Prof .A.K. Swain**, **Prof. D.P. Acharya**, **Prof. S. Maiti** for teaching me different subjects and also helping me how to learn.

I would like to specially thank Mr. Dheeren Kumar Mahapatra for all his help and guidance throughout my research work. I would also like to thank Mrs. Shweta Thomas for her help during my project work.

I would also like to thank all my friends, my classmates, seniors for constant support and encouragement. I am especially indebted to my parents and my brother for their love, sacrifice, and support. I am grateful to my brother for his persistent guidance and support.

Kumari Rosy Pradhan

Abstract

Target detection plays a significant role in many synthetic aperture radar (SAR) applications, ranging from surveillance of military tanks and enemy territories to crop monitoring in agricultural uses. Detection of targets faces two major problems namely, first, how to remotely acquire high resolution images of targets, second, how to efficiently extract information regarding features of clutter-embedded targets. The first problem is addressed by the use of high penetration radar like synthetic aperture radar. The second problem is tackled by efficient algorithms for accurate and fast detection. So far, there are many methods of target detection for SAR imagery available such as CFAR, generalized likelihood ratio test (GLRT) method, multiscale autoregressive method, wavelet transform based method etc. The CFAR method has been extensively used because of its attractive features like simple computation and fast detection of targets. The CFAR algorithm incorporates precise statistical description of background clutter which determines how accurately target detection is achieved.

The primary goal of this project is to investigate the statistical distribution of SAR background clutter from homogeneous and heterogeneous ground areas and analyze suitability of statistical distributions mathematically modelled for SAR clutter. The threshold has to be accurately computed based on statistical distribution so as to efficiently distinguish target from SAR clutter. Several distributions such as lognormal, Weibull, K, KK, G^0, generalized Gamma (GΓD) distributions are considered for clutter amplitude modeling in SAR images. The CFAR detection algorithm based on appropriate background clutter distribution is applied to moving and stationary target acquisition and recognition (MSTAR) images. The experimental results show that, CFAR detector based on GΓD outmatches CFAR detectors based on lognormal, Weibull, K, KK, G^0 distributions in terms of accuracy and computation time.

Keywords: Synthetic aperture radar(SAR); Constant false alarm rate(CFAR); Moving and stationary target acquisition and recognition(MSTAR); Generalized Gamma distribution (GΓD)

Contents

List of Figures

List of Tables

Chapter 1

Introduction

SAR Working Principle

Motivation

Problem Description

Thesis Layout

Chapter 1

Introduction

1.1 SAR Working Principle

SAR is an active imaging system mounted on a moving platform (airplanes), which transmits electromagnetic waves sequentially that are backscattered from earth surface and received back by radar antenna. In SAR, a virtual large aperture is created by moving the small aperture radar along imaginary aperture axis. The basic block diagram of SAR system [20] is shown in Fig. 1.1. Chirp pulse generator produces frequency modulated signal or so called chirp waveform. The transmitted radar pulse from transmitter is received back by SAR antenna which is converted to digital signal by ADC further passed to signal processing unit to generate a raw SAR signal.

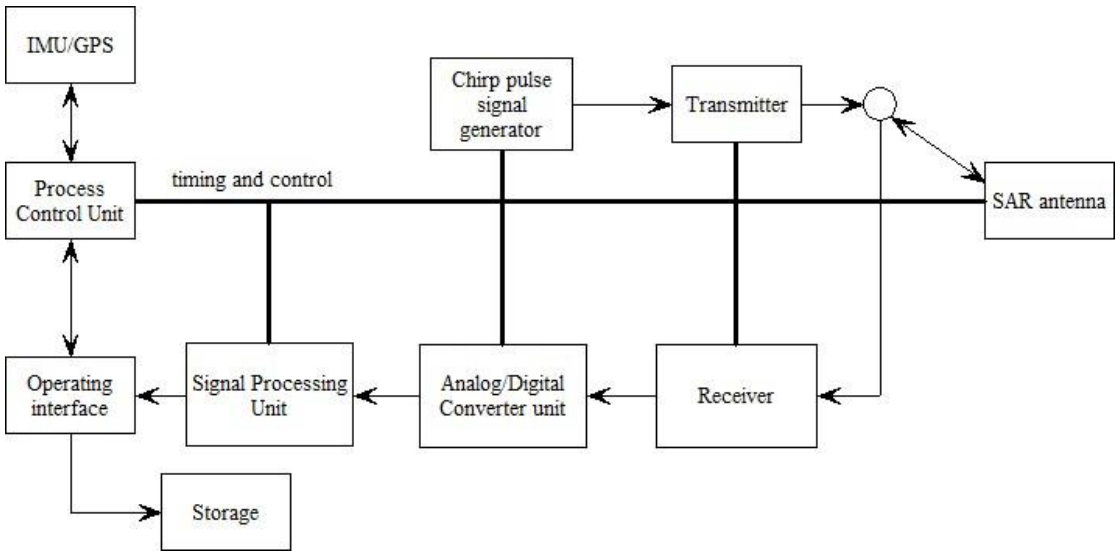

Figure 1.1 Basic block diagram of SAR system

The working of an airborne SAR [14] mounted on an airplane can be explained as follows. Fig. 1.2 illustrates an airborne radar illuminating an area on the earth's surface. The SAR imaging is perpendicular to the aircraft movement. A SAR generates a two-dimensional (2-D) image. The first dimension in the image being range (or cross track) which is a measure of the line-of-sight distance from the radar to the reference target. The resolution and range measurement can be achieved in SAR in the same manner like conventional radars. Typically, range is calculated by measuring the time from transmission of a radar pulse to receiving the echo from a target. And, for the simplest SAR, range resolution can be calculated by the transmitted pulse width. The narrow pulses will provide fine resolution in range.

The second dimension is perpendicular to range is called cross range (or azimuth). The primary advantage of SAR over conventional radar is to produce relatively fine cross range resolution. It can achieve high cross range resolution by realizing a larger aperture with a single large antenna which produces an effect of large array of antennas by focusing the transmitted and received energy into a single sharp beam. The cross range resolution is defined by the sharpness of this transmitted and received beam.

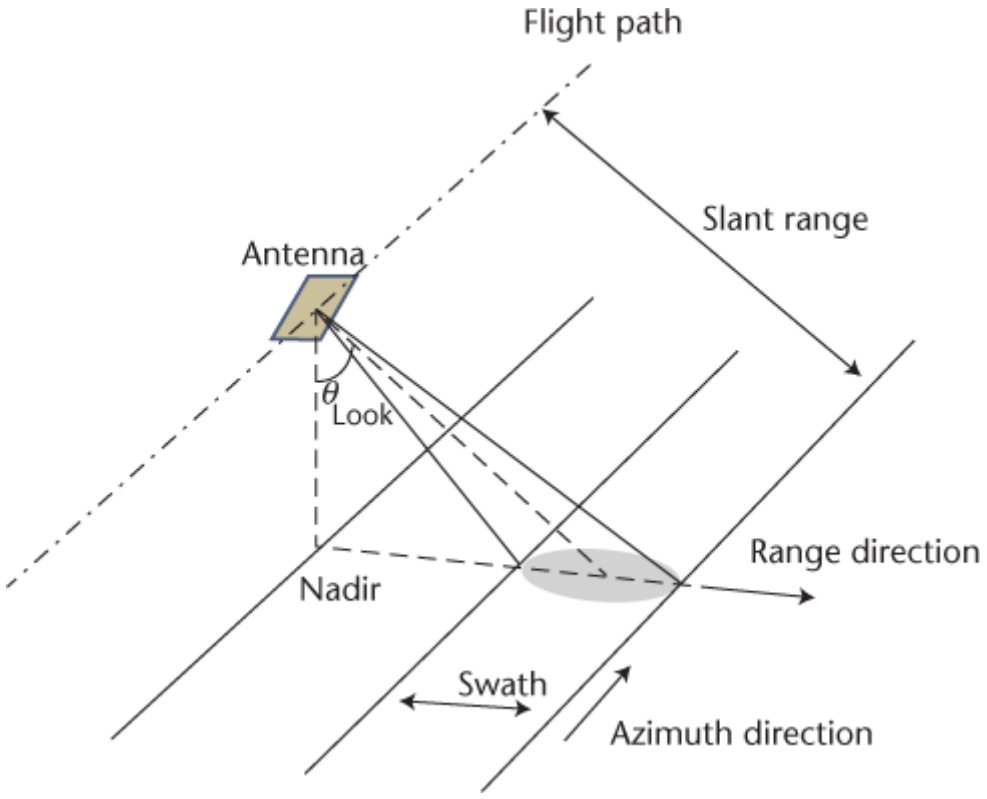

Figure 1.2 SAR acquisition geometry

1.2 Motivation

Military surveillance, environmental tracking, land-resource mapping, necessitates broad-area imaging at high resolutions. This form of imagery is also acquired at night or during inclement weather conditions. SAR provides photographic and optical imaging in any time of day or atmospheric conditions which is a distinct advantage over conventional radars. SAR systems employ long-range propagation characteristics of radar signals as well as the complex information processing capability of modern digital electronics to provide high resolution imagery of targets such as tanks, infantry fighting vehicles, armored personnel carriers, transportation vehicles etc. SAR also ensures unique responses of different terrains and various cultural targets to radar operating frequencies.

The identification and recognition of these targets in SAR images has become intense research area over last couple of decades. Detection of targets faces two major problems namely, first, how to remotely acquire high resolution images of such targets, second, how to efficiently extract information regarding features of clutter-embedded targets. The first problem is addressed by the use of high penetration radar like synthetic aperture radar. The second problem is tackled by efficient algorithms for accurate and fast detection. So far, there are many methods of target detection for SAR image available such as CFAR, Generalized Likelihood Ratio Test (GLRT) method, multiscale autoregressive method, wavelet transform based method etc. The CFAR method has been extensively used because of its attractive features like simple computation and fast detection of targets.

1.3 Problem Description

To perform target detection in SAR imagery, CFAR algorithm is employed. The CFAR target detection algorithm requires exact description about the statistical characteristic of background for maintaining low probability of false alarm. The primary goal of this project is to investigate the statistical distribution of SAR background clutter from homogeneous and heterogeneous ground areas and analyze suitability of statistical distributions mathematically modelled for SAR clutter. The threshold has to be accurately computed based on statistical distribution so as to efficiently distinguish target from SAR clutter.

1.4 Thesis Layout

This thesis consists of a total of six chapters organized as follows:

Chapter 1: This chapter gives a brief introduction about the working of SAR, and problems in target detection in SAR imagery.

Chapter 2: This chapter discusses target detection in SAR and the taxonomy of detection methods.

Chapter 3: This chapter describes about CFAR target detection algorithm, background selection, clutter modeling and detection decision.

Chapter 4: This chapter describes CFAR detection based on different distributions like lognormal, Weibull, K, KK, G^0, $G\Gamma$ distributions**.** It also discusses various parameter estimation methods used for these distributions.

Chapter 5: This chapter gives the implementation of CFAR target detection algorithm and simulation results.

Chapter 6: This chapter discusses about the conclusion and scope of future work.

Chapter 2

Target Detection in SAR

Target Detection

Detection Methods

Chapter 2

Target Detection in SAR

2.1 Target Detection

SAR provides various distinct active remote sensing applications essential for both military and civilian purposes. Target detection is one of major applications in military surveillance, earth resources tracking etc. It also serves as the front-end stage of an automatic target recognition system [15].

The Automatic Target Recognition (ATR) essentially refers to independent or aided detection as well as recognition of targets by processing of radar data from various remote sensing devices. These devices are generally mounted on an airbase or space based systems. Typically, these include SAR, laser radar (LADAR), millimeter-wave (MMW) radar, forward looking infrared (FLIR) or multispectral/hyperspectral sensors. Automatic target recognition is an ability essentially used for surveillance and target tracking of defense weapon systems.

With reference to ATR, three terms of military origins are defined namely, target, clutter, and noise. Its definition depends on the area of application. The target is defined as the objects in focus/interest in the SAR image. While clutter refers to obstacles such as land topologies, forests, terrain, manmade vehicles as well as buildings that are present along with the target. The noise refers to disturbance caused in the reception of echo pulse which is generally caused due to electronic noise present in the SAR sensors and also due to inefficient processing by SAR signal processor.

In Figure 2.1, a basic block diagram for an ATR system [19] is presented. The first stage of an ATR system is considered as a detection stage further followed by an identification stage. The identification stage is more computationally intensive than detection stage. In the ATR

system, the first stage needs to locate regions or areas of interest efficiently. In this stage, essentially manmade objects are located which can be identified as targets. While, in the identification stage, the distinguished regions are further processed so as to determine the type of objects in the identified region.

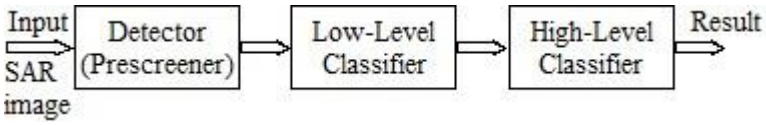

Figure 2.1. An end-to-end SAR-ATR system

The detection stage again can be divided as two separate processes. The first process of detection involves location of pixels that are related to areas of interest. This process is more often called as a focus of attention (FOA) or region segmentation. Further, these unconnected pixels are merged into initial areas of interest. The second process of detection involves extraction of features such as dimensions of regions/areas of interest and any further statistical information from such areas essential to differentiate in an imaged scene. These detected regions are then forwarded to the final stage which is target identification. In this study, the main focus is the detection stage and mostly emphasis is laid upon approaches required for either first or second level detection process.

2.2 Detection Methods

The taxonomy of detection algorithms is divided broadly into three main aspects as reported in the available literature which are single feature based, multi feature based, and expert-system-oriented. The single feature based detection refers to the detecting pixels in SAR image based on a single feature which is generally the pixel brightness usually called as the radar cross-section (RCS). The different modules in the comes in this category. Since, the single feature based detecting method is most common and extensively used in the open literature, it is placed at the base of the taxonomy [19] pyramid in Fig. 2.2. The multi feature and expert system methods are developed from the single feature method.

The multi feature based approach refers to detection based on coalesce of two or more features which are acquired individually from the given SAR data. The characteristics essential which can

be merged for multi feature based detection are multiresolution RCS and fractal dimension along with RCS. Thus, it can be said that taxon takes the previous approach as base and performs refined detection with low probability of false alarms. This approach also involves multiple methods according to the literature.

The expert system oriented taxon is placed at the top of the detection module. It is considered to be most sophisticated and computationally expensive approach. This approach bases detection on the already mentioned approaches and further extends to employ a multistage artificial intelligence(AI). The AI primarily performs detection in the SAR image with the prior knowledge of clutter, target, terrain, forests, imaged scene. This prior knowledge can be extracted from the SAR image through various processed information such as segmentation of image, imaged scene, prior acquired data.

The efficiency of expert-system-oriented approach is limited by complexity-performance tradeoff. Thus, a balance needs to be maintained for complexity tradeoff as well as great caution should be taken to extract the prior data effectively.

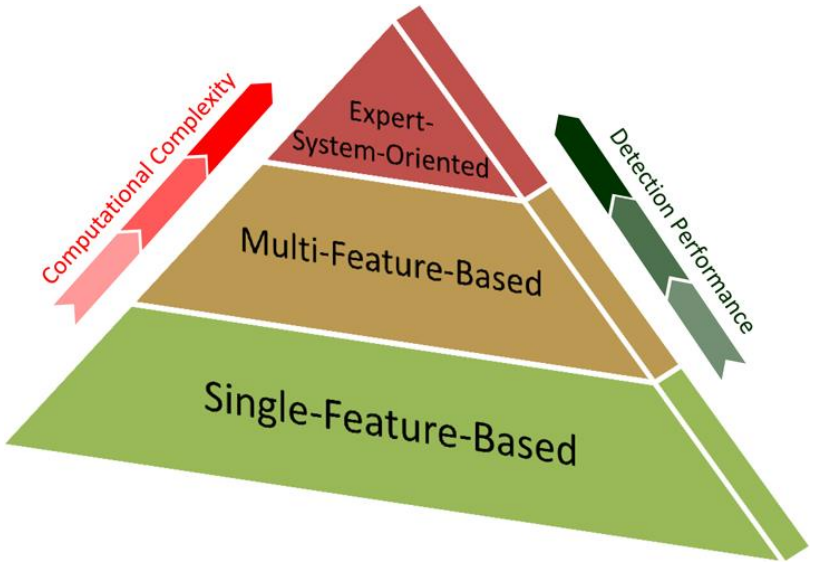

Figure 2.2. Taxonomy of detection module

2.2.1 Single Feature Based Taxon

The single-feature-based detection techniques primarily search for a single feature in the SAR image, typically brightness pixel intensity. The most commonly and widely used single-feature based taxon is CFAR. Even if there exists many CFAR variates, this algorithm is considered as single feature based as it bases its detection search on brightness pixel intensity alone for finding areas of interest. It is clearly mentioned in a number of works according to the available literature. Among all CFAR schemes, Cell Averaging CFAR is the basic method for detecting targets in SAR images. The single feature based method is again divided into sliding window based CFAR and Non-CFAR based method. The sliding window based CFAR algorithm is further explained in Section 3.1.

Apart from CFAR approaches, there are also different methods which prefer not to utilize CFAR. These methods are called as Non-CFAR based method. In such methods, the detection [68] is performed on a multilook SAR image which is formed by cross correlation of two SAR datas through window of relatively smaller size which are slid on entire image. These methods are efficient in reducing speckle noise. According to open literature these detection methods employ genetic programming for advanced applications. Again these methods have been proven to be efficient in detection in one dimensional radar data which essentially involve GLRT. Thus non-CFAR methods are also widespread used similar to CFAR based method.

2.2.2 Multiple Feature Based Taxon

The above mentioned single featured based methods utilized brightness level of pixels so as to distinguish targets from clutter region. But this also limits the efficiency of such methods because in heterogeneous clutter regions or regions with multiple targets the areas of interests are not distinguished effectively. Thus, multifeature based methods comes into picture which pose a solution to this problem.

The multi-feature based methods eliminate the drawback of single feature based method by performing detection based upon mixture of more than two or two features. For proper functioning of these methods, an appropriate method is chosen from already presented single-feature-based method to extract features other than pixel brightness. Furthermore, the methods

coming under multifeature based algorithms are broadly divided into two main approaches i.e. methods that base detection on arbitrarily chosen features by user and methods that are based upon systematic multiresolution analysis. The first method which are based on arbitrary user chosen features differentiate target pixels from background by taking three multistage features altogether. These features are typically obtained parallely from a SAR image and these features are primarily CFAR features, statistical features such as mean and variance, and extended fractal features(EF). Hence, it can be said that this approach is not entirely CFAR.

The second method which relies its detection upon analysis of multiresolution analysis can further be divided into space frequency based and space scale based. The space scale algorithms employ wavelet transforms such as discrete wavelet transform and continuous wavelet transform so as to extract space scale based features. The discrete wavelet transform essentially produces a number of sub-bands which are spatially correlated. The spatially correlated sub-bands differentiates target from clutter by attenuating noise due to background, thus, producing reliably differentiated target signatures. Similarly, methods involving application of continuous wavelet transform on SAR image for detection have advantages over other methods.

The space frequency methods are computationally intensive as compared to space scale based methods. Various space frequency based methods are linear space frequency methods mainly, S-transform, bilinear or quadratic space frequency types for example Cohen's class distributions, Wigner-Ville probability distribution, Wigner probability distribution and pseudo-Wigner-Ville probability distribution, etc.

2.2.3 Expert System Oriented Taxon

Expert-system-oriented detection algorithm is essentially a two-stage or multistage AI based method which performs detection by exploiting knowledge of scene maps, types of target, terrains, clutter. This knowledge is extracted by utilizing context in SAR image. The already mentioned context is broadly identified as existing methods that can extract valuable meaning information of SAR imaged scene, targets, clutter types in the area of interest. These methods can essentially include scene maps, image segmentation, region based segmentation, digital elevation model (DEM), already acquired images, and, geographical information systems(GIS).

The context utilization needed for extraction of prior information can be implemented through unsupervised/ semi-supervised method for region based segmentation of SAR image. Often, image structure maps are extracted from SAR image before application of detection algorithm on images. The appropriate CFAR method is chosen based on these maps which aid CFAR method to select suitable region in imaged scene so that statistics for background modelling are accurately determined. Then, smaller segments are differentiated as targets and larger segments are classified as clutter background. Apart from region based segmentation, annealed based segmentation can also be utilized along with one parameter CFAR.

The various other efficient expert system oriented approaches involve fusion of two or more types of CFAR methods such as Cell Averaging CFAR, Order Statistic CFAR, Greatest of Cell Averaging-CFAR, Smallest of Cell Averaging-CFAR, etc. The individual CFAR methods perform well in specific type of clutter regions depending on the type. The expert system thus employs AI to select appropriate CFAR method depending on the type of clutter background in the imaged scene based on information extracted by context utilization means. The application of expert oriented system for target detection on SAR imagery is an emerging research area.

Chapter 3

CFAR Target Detection Algorithm

Introduction

Background Clutter Selection

Clutter Modeling

Threshold Computation

Detection Decision

Chapter 3

CFAR Target Detection Algorithm

3.1 Introduction

There are many methods of target detection for SAR image available in literature such as GLRT method, extended fractal based method, wavelet transform based method etc. The common method for target detection in SAR imagery is global threshold method which computes a fixed threshold by hit-and-trial method for detection decision [5]. The fixed threshold method has a major problem that if the SAR target image does not have high signal-to-clutter ratio (SCR), almost major target features in the image are lost with considerable clutter remains in the detected image. It is prudent to make use of adaptive threshold algorithms with low computational complexity for effective target detection.

The CFAR algorithm serves as a popular method that is widely used as the front-end stage for various SAR-ATR systems. CFAR detection algorithm has been extensively used because of its following characteristics accurate, easier and faster computation.

These detection methods are very frequently used adaptive threshold methods ensures constant false alarm rate or constant probability of the false alarm.

In this section, CFAR target detection algorithm is described in SAR clutter. The flow of CFAR target detection algorithm [1] is illustrated in Figure.3.1.

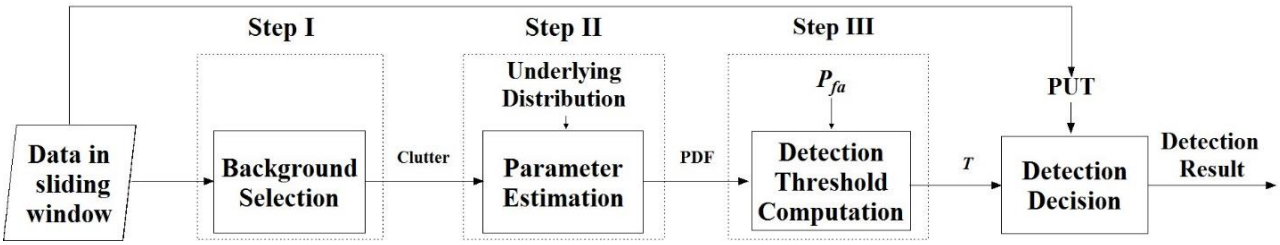

Figure 3.1 CFAR target detection algorithm flow

Four important steps of CFAR target detection includes:

- Background clutter selection
- Parameter estimation
- Adaptive threshold computation
- Detection decision

The following subsections individually explain each block of the detection algorithm in greater detail.

3.2 Background Clutter Selection

In this section, the structure of a square shape sliding window is discussed. The square shaped sliding window is also known as CFAR stencil [19] which is essential for background clutter selection. The improper selection of CFAR stencil can cause loss of target features in detected image. Thus, it is important to adopt certain guidelines for choosing appropriate window size for almost negligible detection loss.

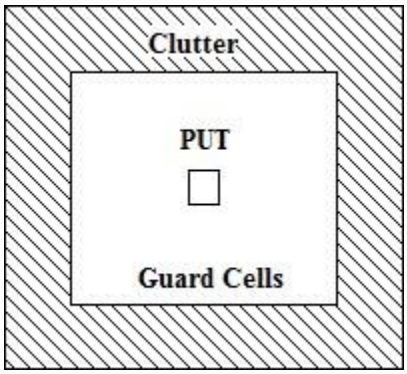

Figure. 3.2 CFAR Stencil

A typical structure of sliding matrix window or CFAR stencil is shown in Figure 3.2 The center pixel of the window is called as PUT. It can be generally a single pixel or a number of pixels depending on the type of CFAR approach. The pixels immediately surrounding the PUT are called guard ring pixels. Excluding the guard ring and PUT, the remaining pixels in the CFAR stencil are called as boundary clutter ring or clutter pixels. The boundary pixels are denoted by the clutter ring.

The choice of such a sliding window shape and size here is only given as an example. The appropriate CFAR stencil size is chosen depending on variety of clutter in SAR image and also size of target. The guard ring features such as shape and size are usually chosen according to geometrical size of the target. Nevertheless, the stencil dimension needs to be chosen with the previously acquired information about target's size which results in detection loss. This is so because targets in SAR images are independent of working situations of SAR and are weakly dependent on geometrical shape of the target. Although such challenges exist it is recommended to choose sliding window size same as about size of smallest object present in the SAR image that needs to be detected. And guard ring size must be same as size of largest object present in SAR image and the boundary ring size or clutter boundary must be large enough so as to accurately estimate clutter statistics essential for threshold computation. The strategies adopted for choosing sliding window size can be summarized as follows:

i. Size of pixel to be tested must be around smallest object's size which need be detected
ii. Size of guard band must be about largest object's size
iii. Size of clutter ring window must be large so as to accurately compute mean and deviation

3.3 Clutter Modeling

The accuracy of CFAR detector is dependent on how well the statistical characteristic of background is described. The method can render a required and constant P_{fa} essential for given entire image only when the underlying chosen distribution describes the background precisely. Thus, it can be said that clutter modeling is of much importance in target detection applications. Because firstly, it results in description of background in SAR images. Next, it gives way to broad research area relating to speckle reduction, detection of sharp edges, segmentation of images,

identification, automatic target detection and recognition in SAR data [19] etc. The clutter modeling is achieved by choosing the appropriate statistical model for the background.

The statistical models [2] for various SAR images are divided into parametric models and non-parametric models. A model which is chosen from several already existing standard distributions for SAR imagery are considered parametric distribution. Having estimated parameters, the optimal distribution is selected which best fits the data obtained by the help of certain quantitative metrics. The nonparametric model does not need prior assumption of certain distributions. Rather, optimal distribution is selected from the training data acquired for a certain time period. The nonparametric models have the advantage of achiever better fitting to real data and also provide more flexibility.

The nonparametric modeling is computationally intensive and also requires large amount of data for computation. Thus it is considered time consuming and unsuitable for a number of applications. Due to these disadvantages parametric modeling is chosen over nonparametric modeling and it is extensively used. The parametric modeling process includes:

1. Analyzing various known standard statistical distributions
2. Parameter estimation: computing unknown parameters of several pdfs
3. Goodness-of-fit test: assessing accuracy of given distributions matching given data

The statistical modeling can again be broadly classified into three main categories:

- Empirical modeling: These distributions are a result of analysis of real data. The different empirical models used for characterizing amplitude or intensity data statistics in SAR image are lognormal, Weibull and Fisher distributions.
- Scattering modeling: The scattering model is based on the conjecture that resolution pixel is mainly dependent on a single scatterer thus, respective amplitude/intensity data exhibits Rician distribution. Thus it can be said that when influential scatterers represent targets which are found in weak clutter the respective image is described by Rician distribution.
- Compound modeling: In compound modeling, a mixture of two distributions is considered for more than two types of heterogeneous clutter scenes in SAR image. The several distributions considered for modeling heterogeneous type of clutter are K, KK, etc. The only concern is that parameter estimation becomes more difficult as the unknown parameters for such modeling increases by several times.

3.3.1 Parameter Estimation

The various techniques used for parameter estimation are maximum likelihood estimation, method of moments, method of log-cumulants.

- Maximum likelihood estimation: The estimator which maximizes likelihood function for a certain value of θ is called maximum likelihood estimator (MLE). Generally, MLE is unbiased hence, shows asymptotic properties. It attains CRLB and has a Gaussian pdf. MLE can be considered as asymptotically efficient that is for large number of data records only, it achieves CRLB. The expression for MLE can be given as follows:

$$\frac{\partial \ln p(x;\theta)}{\partial \theta} = 0 \tag{3.1}$$

- Method of Moments: It is one of the oldest methods for parameter estimation. The procedure of method of moments (MoM) can be summarized as follows:

  Suppose there are n parameters need to be estimated $\theta = (\theta_1, ..., \theta_n)$

  1. Find n population moments, $\hat{\mu}_k$, $k = 1, 2, ..., n$ contain parameters $\theta_1, ..., \theta_n$
  2. Find the corresponding n sample moments, $\hat{m}_k, k = 1, 2, ..., n$. The number of parameters must be equal to the number of sample moments.
  3. Solving the system of equations, $\hat{\mu}_k = \hat{m}_k, k = 1, 2, ..., n$ for finding parameter $\hat{\theta} = (\hat{\theta}_1, ..., \hat{\theta}_n)$

- Method of log-cumulants (MoLC): The moments and cumulants can be deduced by differentiation on logarithmic scale. Thus, log-moments and log-cumulants come into picture. If the moments of a distribution are identical then it can be said that the cumulants of the distribution will also be identical and vice-versa.

3.3.2 Goodness-of-fit Test

The validity of statistical distributions in accordance with given sample data can be quantitatively assessed by a number of methods. The basic requirement of such tests is to search for a model that best matches the analysed data from given SAR image.

The major quantitative metrics for choosing of best fit statistical model are Kolmogorov-Smirnov test, Kullback-Leibler distance, Akaike information criteria, D'Agostino Pearson test, χ^2 matching test and Kuiper test, etc.

- Kullback Leibler divergence: Kullback-Leibler (KL) distance is calculated for choosing appropriate clutter model in terms of histogram matching accuracy between estimated pdfs and data histogram. KL distance quantitatively assesses fitting of an estimated pdf with the data histogram. If KL distance D_{KL} is smaller, it denotes better matching for estimated pdf with given real data histogram. The KL distance D_{KL} for r^{th} gray level can be given in (3.2). The estimated pdf and real data histogram are respectively represented as $h_e(r)$ and $h_d(r)$.

$$D_{KL} = \sum_r \log_e \left(\frac{h_d(r)}{h_e(r)} \right) h_d(r) \tag{3.2}$$

3.4 Threshold Computation

Typically, conventional CFAR detector necessitates a model to describe clutter background and parameters are estimated from the clutter background extracted from boundary ring of the sliding window. The adaptive threshold is computed using the parametric model, $f(x)$ which serves as the underlying distribution chosen from Step II of CFAR algorithm. Let $F(x)$ be the CDF for corresponding underlying distribution, then for a given P_{fa}, adaptive threshold *T* can be calculated from 3.3:

$$P_{fa} = \int_T^\infty f(x)dx = 1 - F(T) \tag{3.3}$$

3.5 Detection Decision

The detection decision is made on PUT by applying appropriate CFAR detection strategy according to the type of clutter regions. The various CFAR strategies based on which detection

decision can be made are described below. As was already mentioned in Section 2.1, the parametric CFAR methods were divided into strategies dependent on clutter modeling and strategies dependent on both clutter and target modeling.

The parametric CFAR algorithms are further divided into 1-parameter and 2-parameter CFAR. The 1-parameter CFAR is basically adopted for CFAR algorithms which consider clutter and estimate the background clutter as an exponential pdf or a Rayleigh pdf. These distributions are characterized by a single parameter which is average/mean and hence, called as 1-parameter CFAR.

In some CFAR methods, the background clutter is modeled by more complex and practically used Weibull distribution, KK-distribution, K- distribution, G^0 distributions. These distributions are parameterized by two parameters which are mean; variance or shape; scale parameters and hence called as 2-parameter CFAR.

Also, there exist methods used to estimate parameters of model so as to calculate threshold for detection decision from the clutter pixels. These are Cell Averaging CFAR (CA-CFAR), Greatest of Cell Averaging CFAR (GOCA-CFAR), Smallest of Cell Averaging CFAR (SOCA-CFAR), Order Statistic CFAR (OS-CFAR) and best linear unbiased estimator CFAR (BLUE-CFAR) are the various strategies.

1-parameter CFAR: The 1-parameter CFAR [19] can be implemented by any one of the algorithms namely, CA-CFAR, SOCA-CFAR, GOCA-CFAR, OS-CFAR. These same strategies are utilized for realizing 2-parameter CFAR. A proper understanding is required for understanding 2-parameter CFAR better.

Fin and Johnson first presented CA-CFAR as the first CFAR method in 1968. The threshold for CA-CFAR is composed of two parts the first part is estimated from clutter pixels and second part can be derived from the corresponding model for a required probability of false alarm. The first part is called Z and second part is called α , threshold scaling factor. The adaptive threshold is calculated as follows:

$$Threshold = \alpha Z \tag{3.4}$$

The CA-CFAR basically calculates ML estimate of arithmetic average of the clutter pixels from sliding window and compares this average with the pixel to be tested for detection. The decision

is made so as to deduce whether PUT is a target pixel or a clutter pixel. This depends on threshold scaling factor α . The detection decision can be made by using the following eqn (3.6):

$$X_{PUT}\begin{cases} > \alpha\hat{\mu}_B \Rightarrow \text{TargetPixel} \\ < \alpha\hat{\mu}_B \Rightarrow \text{ClutterPixel} \end{cases} \tag{3.5}$$

where N denotes total number of clutter pixels in sliding window, $\hat{\mu}_B = \frac{\sum_{i=1}^{N} x_i}{N}$ gives the mean of local background where x_i denotes amplitude of each pixel value in sliding window and X_{PUT} is the amplitude of PUT.

The other two variants of CA-CFAR are SOCA-CFAR and GOCA-CFAR which divide the boundary ring in CFAR stencil into separate windows called lead and lag windows. There are two lead and two lag windows for a CFAR stencil. Based on these windows separate statistics can be estimated. The four mean estimates can be given as follows:

$$mean_{top} = \frac{\sum_{i=1}^{N} x_{i,top}}{N} \tag{3.6}$$

$$mean_{left} = \frac{\sum_{i=1}^{N} x_{i,left}}{N} \tag{3.7}$$

$$mean_{bottom} = \frac{\sum_{i=1}^{N} x_{i,bottom}}{N} \tag{3.8}$$

$$mean_{right} = \frac{\sum_{i=1}^{N} x_{i,right}}{N} \tag{3.9}$$

where $mean_{top}$, $mean_{left}$, $mean_{bottom}$ and $mean_{right}$ are the ML estimates of mean for top, left, bottom, and right windows, respectively in a CFAR stencil , and x_i is the corresponding amplitude value inside each boundary ring.

The detection decision for SOCA-CFAR for amplitude or intensity domain SAR image can be given as per eqn. (3.11):

$$X_{PUT}\begin{cases} > \alpha \min\left(mean_{top}, mean_{bottom}, mean_{left}, mean_{right}\right) \Rightarrow \text{TargetPixel} \\ < \alpha \min\left(mean_{top}, mean_{bottom}, mean_{left}, mean_{right}\right) \Rightarrow \text{ClutterPixel} \end{cases} \tag{3.10}$$

In a similar fashion, for GOCA-CFAR the detection decision can be made as per eqn (3.11):

$$X_{PUT}\begin{cases} > \alpha \max\left(mean_{top}, mean_{bottom}, mean_{left}, mean_{right}\right) \Rightarrow \text{TargetPixel} \\ < \alpha \max\left(mean_{top}, mean_{bottom}, mean_{left}, mean_{right}\right) \Rightarrow \text{ClutterPixel} \end{cases} \tag{3.11}$$

The third variant of CFAR, OS-CFAR is employed so as to detect a number of targets in a SAR image. OS-CFAR basically orders clutter pixels in the leading and lagging windows of boundary ring according to their values. OS-CFAR arranges N clutter pixels from boundary ring in ascending order as follows:

$$x_{(1)} \geq x_{(2)} \geq \ldots\ldots \geq x_{(N)} \tag{3.12}$$

In case of OS-CFAR, the Q' th percentile is chosen instead of mean estimate in CA-CFAR. Hence, detection decision is made as per eqn. (3.14):

$$X_{PUT}\begin{cases} > \alpha x_{(Q)} \Rightarrow \text{TargetPixel} \\ < \alpha x_{(Q)} \Rightarrow \text{ClutterPixel} \end{cases} \tag{3.13}$$

2-parameter CFAR: The more practically used CFAR detection decision unlike 1-parameter CFAR distribution models are 2-parameter CFAR. These 2-parameter distribution models are basically parameterized by two parameters mean; variance or scale; shape parameters estimated from clutter pixels in sliding window. The 2-parameter CFAR typically considers either lognormal distribution or Weibull distribution as distribution models for clutter background. The more complex 2-parameter distributions such as K distribution, G^0 distribution and β' distribution are generally used for high-resolution SAR imagery. The two-parameter CA-CFAR bases its detection decision on the log detector which can be given as follows:

$$X_{PUT}\begin{cases} > \hat{\mu}_B + \hat{\sigma}_B \alpha \Rightarrow \text{TargetPixel} \\ < \hat{\mu}_B + \hat{\sigma}_B \alpha \Rightarrow \text{ClutterPixel} \end{cases} \tag{3.14}$$

where α is considered as the threshold scaling factor obtained from an appropriate model for the clutter in SAR image for a given P_{fa} ,

$\hat{\mu}_B = \frac{\sum_{i=1}^{N} x_i}{N}$ and $\hat{\sigma}_B = \sqrt{\frac{\sum_{i=1}^{N} \left(x_i - \hat{\mu}_B\right)^2}{N}}$ are mean and standard deviation of local background.

Typically, PUT is considered to be a single pixel. But in certain cases if more than a single pixel is considered, then PUT is considered as the MLE of the arithmetic mean such that

$$\bar{X}_{PUT} = \frac{\sum_{i=1}^{M} x_i}{M} \tag{3.15}$$

where M is the total number of pixels in the PUT and x_i is amplitude value corresponding to each pixel in the PUT.

Chapter 4

CFAR Detectors Based on Various Distributions

Lognormal Distribution

Weibull Distribution

K Distribution

KK Distribution

G^0 Distribution

GΓD

Chapter 4

CFAR Detectors Based on Various Distributions

4.1 Lognormal Distribution

Goodman presented the statistical model for single polarization SAR data. He stated that the background clutter signal in given SAR data can be expressed as a superposition of random contributions from various scatterers within radar illumination area based on assumption that the illuminated area is considerably smaller than the frequency. The clutter amplitudes can be assumed to be independent random variables and N is considered large thus, as a consequence of the central limit theorem, the backscattered field E_s possesses Gaussian distribution. Then, the amplitude of the backscattered field E_s shows Rayleigh distribution features. The probability density function of Rayleigh distributed random variable x with parameter σ is given as

$$f(x;\sigma) = \frac{x}{\sigma}\exp(-\frac{x^2}{2\sigma}), x > 0 \quad (4.1)$$

where x represents amplitude of clutter and σ is scale parameter of the distribution. The afore mentioned model fits the amplitude distribution of clutter extracted from natural radar clutter textures with low resolutions. The clutter characteristics deviates from Rayleigh behavior for high resolution SAR images and also for low grazing angles. For high resolution radars like SAR the models having longer tails than Rayleigh pdf matches clutter amplitude better. Thus, lognormal was given as an alternative to Rayleigh distribution.

The lognormal distribution describes natural phenomena better as mentioned in open literature. Several natural growth processes are driven by accumulation of small percentage changes. On a log scale, these become additive. When the effect of any one change is insignificant, the central limit theorem states that the distribution of their sum is more nearly normal than that of the summands. Though if the standard deviation is sufficiently small, the normal distribution can be considered an approximation when back-transformed onto original scale. It makes the distribution approximately lognormal. The main feature of this distribution its long tail. In, high resolution radar, return signals possess many spikes. It is found that the clutter amplitude has a longer tail in comparison to Rayleigh distribution. Lognormal distribution is heavy-tailed and is suited for modeling heterogeneous areas. The pdf of lognormal distribution is given as

$$f(x;[\kappa,\eta]) = \frac{1}{\sqrt{2\pi}\kappa x}\exp(-\frac{(\ln x-\eta)^2}{2\kappa^2}), x>0 \tag{4.2}$$

where κ and η denote variance and mean parameter, respectively.

Parameter Estimation: The MLE is employed for parameter estimation of this parametric pdf. In this method, the parameters are estimated by expressions derived from (4.2). The obtained expressions are given as follows:

$$\hat{\eta} = \frac{1}{N}\sum_{i=1}^{N}\ln x_i \tag{4.3}$$

$$\hat{\kappa} = \frac{1}{N}\sum_{i=1}^{N}(\ln x_i-\eta)^2 \tag{4.4}$$

The MoLC is further employed for parameter estimation of this parametric pdfs. In this method, the parameters are estimated by solving a system of equations of log-cumulants statistics. The first and second log-cumulants of lognormal distribution given in (4.5) and (4.6) are computed as

$$\hat{k}_1 = \eta \tag{4.5}$$

$$\hat{k}_2 = \kappa^2 \tag{4.6}$$

The parameter estimate of lognormal distribution can be obtained by solving system of equations given in (4.7) and (4.8) where the first-kind cumulants and second-kind cumulants are computed from real data as

$$\hat{\hat{k}}_1 = \frac{1}{N}\sum_{i=1}^{N}[\log(r_i)] \tag{4.7}$$

$$\hat{\hat{k}}_i = \frac{1}{N}\sum_{i=2}^{N}[(\log(r_i) - \hat{\hat{k}}_1)^n] \tag{4.8}$$

where $i = 2$ and N is the number of independent data samples used for estimation of parameters and r_i is the amplitude of clutter pixel.

Threshold Computation: The adaptive threshold is computed using the parametric model for Weibull pdf $f(x)$ that suitably fits the local background clutter around the PUT in the sliding window. Let $F(x)$ be the corresponding cumulative distribution function (cdf), then for a desired P_{fa}, adaptive threshold *T* can be obtained as

$$P_{fa} = \int_{T}^{\infty} f(x)dx = 1 - F(T) \tag{4.9}$$

The adaptive threshold, T_{Lgn} of CFAR algorithm based on lognormal distribution can be obtained by plugging (4.2) into (4.9). The obtained expressions may be given as

$$P_{fa} = \frac{1}{2} - \frac{1}{2} erf\left(\frac{\ln T_{Lgn} - \eta}{\sqrt{2}\kappa}\right) \tag{4.10}$$

where $erf(.)$ denotes error function.

The error function can be defined as follows:

$$erf(x) = \frac{2}{\sqrt{\pi}}\int_{0}^{x} \exp(-t^2)dt \tag{4.11}$$

Detection Decision: The detection decision is made on PUT by applying 2-parameter CFAR detection strategy which may be given as

$$y_t \begin{cases} > \mu_b + \sigma_b T_{Lgn} \Rightarrow \text{TargetPixel} \\ < \mu_b + \sigma_b T_{Lgn} \Rightarrow \text{ClutterPixel} \end{cases} \tag{4.12}$$

where y_t represents the clutter amplitude of PUT, μ_b and σ_b denotes sample mean and standard deviation computed from clutter data of the local background, T_{Lgn} denotes adaptive threshold for lognormal distributed clutter respectively.

4.2 Weibull Distribution

Weibull distribution is suitable to model areas with low heterogeneity. The location parameter is not used in case of Weibull pdf [16] and its value is set to zero. The distribution expression reduces to 2-parameter Weibull pdf when such a situation arises. Another form of Weibull distribution also exists known as 1-parameter Weibull pdf. It is of the same form as 2-parameter Weibull pdf with a single difference that scale parameter η should be determined beforehand. Thus, only shape parameter κ needs to be estimated for small data sets. The analyst needs to have an accurate and justifiable estimate for shape parameter κ for 1-parameter Weibull distribution. The pdf for Weibull distribution is given as

$$f(x;[\kappa,\eta]) = \frac{\kappa}{\eta^{\kappa}}(x)^{\kappa-1}\exp\left[-\left(\frac{x}{\eta}\right)^{\kappa}\right], x > 0 \tag{4.13}$$

where κ and η denote shape and scale parameter, respectively.

Parameter Estimation: The MLE is employed for parameter estimation of Weibull distribution. In this method, the parameters are estimated by solving the following expression given for $\hat{\kappa}$

$$\frac{\sum_{i=1}^{N} x_i^{\hat{\kappa}} \ln x_i}{\sum_{i=1}^{N} x_i^{\hat{\kappa}}} - \frac{1}{N}\sum_{i=1}^{N}\ln x_i - \frac{1}{\hat{\kappa}} = 0 \tag{4.14}$$

This equation is not a closed form expression hence, solved by Newton-Raphson method. Having solved for $\hat{\kappa}$, the expression for $\hat{\eta}$ can be given as follows:

$$\hat{\kappa} = \left(\frac{1}{N}\sum_{i=1}^{N} x_i^{\hat{\eta}}\right)^{\hat{\eta}} \tag{4.15}$$

The MoLC is also employed for parameter estimation of shape and scale parameters of Weibull pdf. In this method, the parameters are estimated by solving a system of equations of log-cumulants statistics (4.14), (4.15). The first and second log-cumulants of Weibull distribution already mentioned in (4.16) and (4.17).

$$\hat{k}_1 = \log\eta + \psi(1)\kappa^{-1} \tag{4.16}$$

$$\hat{k}_2 = \psi(1,1)\kappa^{-2} \tag{4.17}$$

The parameter estimate of lognormal distribution can be obtained by solving system of equations given in (4.16) and (4.17) where the first-kind cumulants and second-kind cumulants are computed from real data as

$$\hat{\hat{k}}_1 = \frac{1}{N}\sum_{i=1}^{N}[\log(r_i)] \tag{4.18}$$

$$\hat{\hat{k}}_i = \frac{1}{N}\sum_{i=2}^{N}[(\log(r_i) - \hat{\hat{k}}_1)^n] \tag{4.19}$$

where $i = 2$ and N is the number of independent data samples used for estimation of parameters and r_i is the amplitude of clutter pixel.

Threshold Computation: The adaptive threshold is computed using the parametric model for Weibull pdf $f(x)$ that suitably fits the local background clutter around the PUT in the sliding window. Let $F(x)$ be the corresponding cdf, then for a desired P_{fa}, adaptive threshold *T* can be obtained from (4.9).

The adaptive threshold, T_{Wbl} for CFAR algorithm based on Weibull distribution can be obtained by plugging (4.13) into (4.9). The obtained expressions may be given as

$$T_{Wbl} = \left(\ln\frac{1}{P_{fa}}\right)^{1/\kappa}\eta \tag{4.20}$$

Detection Decision: The detection decision is made on PUT by applying 2-parameter CFAR detection strategy which may be given as

$$y_t \begin{cases} > \mu_b + \sigma_b T_{wbl} \Rightarrow \text{TargetPixel} \\ < \mu_b + \sigma_b T_{wbl} \Rightarrow \text{ClutterPixel} \end{cases} \tag{4.21}$$

where y_t represents the clutter amplitude of PUT , μ_b and σ_b denotes sample mean and standard deviation computed from clutter data of the local background, T_{Wbl} denotes adaptive threshold for Weibull distributed clutter respectively.

4.3 K Distribution

K-distribution [3] has been widely used for modeling the radar clutter envelope in radar systems for many signal processing applications. K-distribution is considered as a suitable model for fitting ground clutter at high resolution. It is also chosen as underlying distribution suitable for pure sea clutter and land clutter with many spikes.

The pdf for K-distribution [5] is given as:

$$f(x;[b,v]) = \frac{2}{\Gamma(v+1)}\left(\frac{x}{2b}\right)^{v+1} K_v\left(\frac{x}{b}\right) \tag{4.22}$$

where b is scaling parameter, v is shape parameter, Γ is standard gamma function and K_v is modified Bessel function of second kind of order v.

Parameter Estimation: The MLE can be used to estimate parameters of K pdf. The ML estimates are asymptotically efficient and are computationally expensive to be used in real-time systems. The method of moments leads to accurate parameter estimates however, computational expensive numerical methods are involved in solving nonlinear equations. Hence, method of moments is also not an efficient method for parameter estimation of K distribution. The next approach mentioned in literature used for parameter estimation is higher order and fractional sample moments. It is based on calculation of fourth and second-order moments. This method performs well for a large number of samples. But good performance cannot be achieved for smaller amount of available data. The assumption of local stationarity can only be made when sample size is small. Hence, methods which are computationally realizable in real time should give accurate parameter estimation even for a small data sample. The shape parameter v can be estimated independently by using higher order statistics and sample moments [4]. The expression for shape parameter estimate v is given as follows:

$$v = \frac{4 - \frac{\hat{\mu}_4}{\hat{\mu}_2^2}}{\frac{\hat{\mu}_4}{\hat{\mu}_2^2} - 2} \tag{4.23}$$

Having determined v, the scale parameter b is estimated as per the given expression in (39)

$$b = \frac{\hat{\mu}_1 \Gamma(v+1)}{\sqrt{\pi}\Gamma(v+1.5)} \tag{4.24}$$

The fourth and second order moments used in (4.23) and (4.24) can be given as follows:

$$\hat{\mu}_n = \frac{1}{N}\sum_{i=1}^{N} x_i^n \tag{4.25}$$

Threshold Computation: The adaptive threshold is computed using the parametric model, $f(x)$ which serves as the underlying distribution chosen from Step II of CFAR algorithm. Let $F(x)$ be the cdf for corresponding underlying distribution, then for a given P_{fa}, adaptive threshold *T* can be obtained from (4.9).

The adaptive threshold, T_{Kpdf} for CFAR algorithm for the background considered K-distribution can be obtained by plugging (4.22) into (4.9) which is given as:

$$P_{fa} = \frac{2}{\Gamma(v+1)}\left(\frac{T_{Kpdf}}{2b}\right)^{v+1} K_{v+1}\left(\frac{T_{Kpdf}}{b}\right) \tag{4.26}$$

The adaptive threshold for K-distribution can be calculated by solving Eqn. (4.26) by numerical method such as Newton-Raphson method.

Detection Decision: The detection decision is made on PUT by applying 2-parameter CFAR detection strategy which may be given as

$$y_t \begin{cases} > \mu_b + \sigma_b T_{Kpdf} \Rightarrow \text{TargetPixel} \\ < \mu_b + \sigma_b T_{Kpdf} \Rightarrow \text{ClutterPixel} \end{cases} \tag{4.27}$$

where y_t represents the clutter amplitude of PUT, μ_b and σ_b denotes sample mean and standard deviation computed from clutter data of the local background, T_{Kpdf} denotes adaptive threshold respectively.

4.4 KK Distribution

The K distribution is a suitable model for high resolution sea clutter regions at a low grazing angle as mentioned in the open literature. The K distribution performs well when these sea clutter regions are subjected to shadowing, multipath propagation and ducting. The clutter returns suffer from

scattering due to whitecaps at higher grazing angles and also by Bragg scattering from rough sea surface. Hence, conventional K distribution is no more a suitable distribution for pure sea clutter because of presence of severe spikes.

The K_A pdf has a major advantage that it improves fitting between sea clutter and chosen distribution in tail region especially. The distribution chosen for sea clutter with many spikes deviates from conventional K distribution in tail region. The main disadvantage of K_A distribution is it cant be represented in closed form expression. The computation of its pdf and cdf is complex because it needs to be numerically computed. Thus, the calculation of adaptive threshold essential for CFAR target detection algorithm becomes significantly difficult.

The KK distribution [12] is presented as an alternative to K distribution which can model sea clutter in high resolution images. The Bragg scattering and whitecap scattering both are considered to be K distributed and spikes are also considered K distributed.

The KK distribution is a mixture of two K distributions. The pdf of KK distribution is given as follows:

$$f_{KK}(x) = (1-k) f_{K_1}(x; v_1, b_1) + k f_{K_2}(x; v_2, b_2), x > 0 \tag{4.28}$$

where f_{K_1} and f_{K_2} are two K distribution with specified parameters characterized by the densities

$$f_{K_j}(x; v_j, b_j) = \frac{2}{b_j \Gamma(v_j)} \left(\frac{x}{2b_j} \right)^{v_j} K_{v_j - 1} \left(\frac{x}{b_j} \right), x \geq 0, v_j \geq 0, b_j \geq 0, j = 1, 2 \tag{4.29}$$

where v_j , b_j are the shape and scale parameters, respectively, $K_{v_j-1}(.)$ modified Bessel function of second kind of order v_j and Γ is standard gamma function. The first K distribution f_{K_1} in (4.28), which is called K_1 component here, denotes the Bragg/whitecap scatters, and the second K distribution f_{K_2} in (4.28), which is called K_2 component, represents the spike component. k is called as mixing coefficient and typically $k \varepsilon [0,1]$. If k = 0, $f_{KK}(x)$ = f_K and KK distribution reduces to standard K distribution. The spike component is not considered in such a case.

The cdf of KK distribution can be derived as follows

$$F_{KK}(x) = (1-k) F_{K_1}(x) + k F_{K_2}(x), x > 0 \tag{4.30}$$

$$F_{KK}(x) = (1-k)\left[1 - \frac{2}{\Gamma(v_1)}\left(\frac{x}{2b_1}\right)^{v_1} K_{v_1}\left(\frac{x}{b_1}\right)\right] + k\left[1 - \frac{2}{\Gamma(v_2)}\left(\frac{x}{2b_2}\right)^{v_2} K_{v_2}\left(\frac{x}{b_2}\right)\right], x > 0 \quad (4.31)$$

where $F_{K_1}(x)$ and $F_{K_2}(x)$ represent cdf of the component K_1 and K_2, respectively.

Parameter Estimation: The effective modeling of clutter involves parameter estimation of assumed pdf that best matches the given data. The sea clutter model typically deviates from standard K distribution at 1-cdf equal to about 10^{-3} or higher. Thus it can be assumed that the shape parameter Since the sea clutter distribution usually departs from the K distribution at 1-cdf equal to, it is rational to assume the shape parameter v and the mean intensity of Bragg/whitecap scatterers of KK distribution are same as parameters of K distribution. The shape parameter v can be estimated independently by using higher order statistics and sample moments. The expression for shape parameter estimate v is given as follows:

$$v = \frac{4 - \frac{\hat{\mu}_4}{\hat{\mu}_2^2}}{\frac{\hat{\mu}_4}{\hat{\mu}_2^2} - 2} \quad (4.32)$$

Having determined v, the scale parameter b is estimated as per the given expression in (4.32)

$$b = \frac{\hat{\mu}_1 \Gamma(v+1)}{\sqrt{\pi}\Gamma(v+1.5)} \quad (4.33)$$

The fourth and second order moments used in (4.32) and (4.33) can be given as follows:

$$\hat{\mu}_n = \frac{1}{N}\sum_{i=1}^{N} x_i^n \quad (4.34)$$

The semi-experiential algorithm [12] was presented by Dong for parameter estimation of KK distribution for modeling high resolution clutter data. The two general hypotheses considered in this method are given as follows:

1) shape parameters of the both K components are assumed to be equal, i.e., $v_1 = v_2$
2) mixing coefficient k is selected experimentally;

The five parameters of KK distribution can be estimated with the aforementioned assumptions. The estimation process is mentioned as following:

1) Choose mixing coefficient k experimentally according to statistical character of given SAR clutter data.

2) Parameters $\hat{v}$, $\hat{b}$ of the K_1 distribution are estimated using (4.32) & (4.33) from the data set and assign them to the component of KK directly, i.e., $v_1 = v_2 = \hat{v}$, $b_1 = \hat{b}$.

3) Scale parameter b_2 of K_2 component is estimated by making use of the discrepancies of the CDF of K and KK distribution.

The mixing coefficient is chosen as k=0.01 according to characteristic of the clutter data. And, it is proved in literature that this algorithm is effective. The mixing coefficient k is very hard to be chosen accurately and quickly for radar clutter data under different conditions. There is no efficient method to choose k accurately. If the mixing coefficient k becomes larger, discrepancies increase between KK distribution and its K_1 component. For the cases when k is not as small as 0.01, it is not justifiable to assign the parameter values of K distribution to the K_1 component as mentioned earlier in step (2). Thus, the mixing coefficient is carefully selected as 0.01.

Threshold Computation: The adaptive threshold is computed using the parametric model, $f(x)$ which serves as the underlying distribution chosen from Step II of CFAR algorithm. Let $F(x)$ be the cdf for corresponding underlying distribution, then for a given P_{fa}, adaptive threshold *T* can be obtained from (4.9).

The adaptive threshold for KK-distribution can be given by plugging (4.28) into (4.9):

$$P_{fa} = \frac{2-2k}{\Gamma(v_1)}\left(\frac{T_{KKpdf}}{2b_1}\right)^{v_1} K_{v_1}\left(\frac{T_{KKpdf}}{b_1}\right) + \frac{2k}{\Gamma(v_2)}\left(\frac{T_{KKpdf}}{2b_2}\right)^{v_2} K_{v_2}\left(\frac{T_{KKpdf}}{b_2}\right) \tag{4.35}$$

The threshold can be calculated by solving (4.35) by numerical method such as Newton-Raphson method.

Detection Decision: The detection decision is made on PUT by applying 2-parameter CFAR detection strategy which may be given as

$$y_t \begin{cases} > \mu_b + \sigma_b T_{KKpdf} \Rightarrow \text{TargetPixel} \\ < \mu_b + \sigma_b T_{KKpdf} \Rightarrow \text{ClutterPixel} \end{cases} \tag{4.36}$$

where y_t represents the clutter amplitude of PUT, μ_b and σ_b denotes sample mean and standard deviation computed from clutter data of the local background, T_{KKpdf} denotes adaptive threshold respectively.

4.5 G^0 Distribution

The G^0 distribution [7] can model variety of clutter regions namely, extremely heterogeneous regions such as urban areas, moderately heterogeneous regions such as dense forests and homogeneous regions such as deserts and crops. The G^0distribution is characterized by parameters such as the number of looks (L), a scale parameter (γ) and a roughness parameter (α).The pdf of G^0distribution is given in eqn. (4.37). The G^0distribution has same interpretational features as K distribution. The scale parameter γ denotes relative power between incident and reflected signals. The parameter α is related to roughness of target and holds great importance in many detection algorithms. The roughness parameter α is used to make deductions about the land types present in a given SAR image.

$$f(x;[n,\alpha,\gamma]) = \frac{2n^n\Gamma(n-\alpha)\gamma^{-\alpha}x^{2n-1}}{\Gamma(n)\Gamma(-\alpha)(\gamma+nx^2)^{n-\alpha}}, x>0 \tag{4.37}$$

The G^0 distribution for a single-look image reduces to

$$f(x;[\alpha,\gamma]) = \frac{-2\alpha\gamma^{-\alpha}x}{(\gamma+x^2)^{1-\alpha}}, x>0 \tag{4.38}$$

Parameter Estimation: The G^0distribution has been analyzed for modeling the background clutter of the SAR target image. The parameters of the G^0distribution are estimated by MLE and also MoM [7]. The MoM is considered to be an optimal method for modeling of large data samples. The ML estimates of the parameters for G^0distribution can be given as,

$$\hat{\alpha} = -\frac{1}{\frac{1}{N}\sum_{i=1}^{N}\ln(1+\frac{x_i^2}{\hat{\gamma}})} \tag{4.39}$$

$$\hat{\gamma} = \left(1+\frac{1}{\frac{1}{N}\sum_{i=1}^{N}\ln\left(1+\frac{x_i^2}{\hat{\gamma}}\right)}\right)\times\left(\frac{1}{N}\sum_{i=1}^{N}\frac{x_i^2}{1+\frac{x_i^2}{\hat{\gamma}}}\right) \tag{4.40}$$

The MoM is intensively used in remote sensing applications. It is computationally inexpensive and implementable in most real-time situations. The roughness parameter $\alpha < -1/2$ is assumed so as to have random variables with finite mean. The j^{th} order moment is defined as below:

$$m_{j,N} = \left(\frac{1}{N} \sum_{i=1}^{N} x_i^{\,j} \right) \tag{4.41}$$

Putting $j = 1/2, 1$ the half and first order moments are given as shown in eqn. (4.42) and eqn. (4.43)

$$m_{1/2,N} = \left(\frac{1}{N} \sum_{i=1}^{N} x_i^{1/2} \right) \tag{4.42}$$

$$m_{1,N} = \left(\frac{1}{N} \sum_{i=1}^{N} x_i \right) \tag{4.43}$$

Using (4.42) and (4.43), half and first order moments estimators for α and γ are denoted by $\hat{\alpha}$ and $\hat{\gamma}$ which can be calculated as follows:

$$m_{1/2,N} = \left(\hat{\gamma}^{1/4} \frac{\Gamma\left(-\hat{\alpha} - \frac{1}{4}\right)\Gamma\left(\frac{1}{4}\right)}{4\Gamma\left(-\hat{\alpha}\right)} \right) \tag{4.44}$$

$$m_{1,N} = \left(\hat{\gamma}^{1/2} \frac{\sqrt{\pi}\Gamma\left(-\hat{\alpha} - \frac{1}{2}\right)}{2\Gamma\left(-\hat{\alpha}\right)} \right) \tag{4.45}$$

The parameters are estimated by solving (4.44) through numerical method like Newton-Raphson method with an initial guess for both parameters. Having calculated one parameter, the next parameter is calculated from (4.45).

Threshold Computation: The adaptive threshold for G^0 distribution can be calculated by plugging (4.38) into (4.9). The obtained expression is given as:

$$T_{G^0} = \sqrt{((P_{fa})^{1/\hat{\alpha}} - 1)\hat{\gamma}} \tag{4.46}$$

Detection Decision: The detection decision is made on PUT by applying 2-parameter CFAR detection strategy which may be given as

$$y_t \begin{cases} > \mu_b + \sigma_b T_{G^0} \Rightarrow \text{TargetPixel} \\ < \mu_b + \sigma_b T_{G^0} \Rightarrow \text{ClutterPixel} \end{cases} \tag{4.47}$$

where y_t represents the clutter amplitude of PUT , μ_b and σ_b denotes sample mean and standard deviation computed from clutter data of the local background, T_{G^0} denotes adaptive threshold respectively.

4.6 GΓD

A GΓD can be used as underlying distribution for various clutter scenes of SAR high-resolution images at high grazing angles. It has been validated in literature that this distribution performs better than several other standard distributions for many different types of clutter cases. Stacy first presented GΓD [9] and it has been extensively used in many fields. The conventional GΓD is a continuous probability distribution with three parameters. It is considered to be a generalization of the two-parameter standard gamma distribution.

Stacy's model is generalized to present a new GΓD, which is given by

$$f(x;[k,v,\sigma]) = \frac{|v|k^k}{\sigma\Gamma(k)}\left(\frac{x}{\sigma}\right)^{kv-1}\exp\left(-k\left(\frac{x}{\sigma}\right)^{v}\right) \tag{4.48}$$

Parameter Estimation: By employing MoLC [10], the estimates of parameters for GΓD are found as:

$$\hat{k} = -\frac{a_1}{3a_0} + \sqrt[3]{-\frac{q}{2} + \sqrt{\left[\frac{q}{2}\right]^2 + \left[\frac{p}{3}\right]^3}} + \sqrt[3]{-\frac{q}{2} - \sqrt{\left[\frac{q}{2}\right]^2 + \left[\frac{p}{3}\right]^3}} \tag{4.49}$$

$$\hat{v} = \operatorname{sgn}\left(-\tilde{k}_3\right)\sqrt{\frac{\psi(1,\hat{k})}{\tilde{k}_2}} \tag{4.50}$$

$$\hat{\sigma} = \exp\left\{\tilde{k}_1 - \left(\frac{\psi(\hat{k}) - \ln\hat{k}}{\hat{v}}\right)\right\} \tag{4.51}$$

where a_0, a_1, a_2, a_3, p ,q are given as follows

$$a_0 = 8\tilde{k}_3^2 \tag{4.52}$$

$$a_1 = 4(3\tilde{k}_3^2 - 2\tilde{k}_2^3) \tag{4.53}$$

$$a_2 = 2(3\tilde{k}_3^2 - 8\tilde{k}_2^3) \tag{4.54}$$

$$a_3 = \tilde{k}_3^2 - 8\tilde{k}_2^3 \tag{4.55}$$

$$p = \frac{3a_0a_2 - a_1^2}{3a_0^2} \tag{4.56}$$

$$q = \frac{2a_1^3 - 9a_0a_1a_2 + 27a_0^2a_3}{27a_0^3} \tag{4.57}$$

The $\psi(t)$ and $\psi(n,t)$ used in (4.50) and (4.51) are mentioned as follows $\psi(t) = \frac{d}{dt}(\log\Gamma(t))$ is Digamma function and $\psi(n,t) = \frac{d^{n+1}}{dt^{n+1}}(\log\Gamma(t))$ is Polygamma function.

The first three log-cumulants $\tilde{k}_1$, $\tilde{k}_2$, $\tilde{k}_3$ used in (4.50)-(4.57) are calculated from sample data as follows [18]:

$$\tilde{k}_1 = \frac{1}{N}\sum_{i=1}^{N}\ln(x_i) \tag{4.58}$$

$$\tilde{k}_2 = \frac{1}{N}\sum_{i=1}^{N}(\ln(x_i) - \tilde{k}_1)^2 \tag{4.59}$$

$$\tilde{k}_3 = \frac{1}{N}\sum_{i=1}^{N}(\ln(x_i) - \tilde{k}_1)^3 \tag{4.60}$$

Threshold Computation: The CDF for GΓD distribution can be given as follows:

$$F(x) = \begin{Bmatrix} \frac{1}{\Gamma(k)} \int_0^{k\left(\frac{x}{\sigma}\right)^v} z^{k-1}\exp(-z)dz, v > 0 \\ \frac{1}{\Gamma(k)} \int_{k\left(\frac{x}{\sigma}\right)^v}^{\infty} z^{k-1}\exp(-z)dz, v < 0 \end{Bmatrix} \tag{4.61}$$

The eqn. (4.63) can be represented as:

$$F(x) = \begin{Bmatrix} Q\left(k\left(x/\sigma\right)^v, k\right), v > 0 \\ 1 - Q\left(k\left(x/\sigma\right)^v, k\right), v < 0 \end{Bmatrix} \tag{4.62}$$

where $Q(x,a)$ is incomplete gamma function[11].

$$Q(x,a)=\frac{1}{\Gamma(a)}\int_0^x z^{a-1}\exp(-z)dz \tag{4.63}$$

The adaptive threshold for GГD distribution[1] can be calculated by solving Eqn. (4.9):

$$T_{G\Gamma D}=\begin{Bmatrix}\sigma\left\{\frac{1}{k}Q_{INV}\left(1-P_{fa},k\right)\right\}^{\frac{1}{v}},v>0\\ \sigma\left\{\frac{1}{k}Q_{INV}\left(P_{fa},k\right)\right\}^{\frac{1}{v}},v<0\end{Bmatrix} \tag{4.64}$$

Detection Decision: The detection decision is made on PUT by applying two parameter CFAR detection strategy which may be given as

$$y_t\begin{cases}>\mu_b+\sigma_b T_{G\Gamma D}\Rightarrow \text{TargetPixel}\\ <\mu_b+\sigma_b T_{G\Gamma D}\Rightarrow \text{ClutterPixel}\end{cases} \tag{4.65}$$

where y_t represents the clutter amplitude of pixel under test (PUT) , μ_b and σ_b denotes sample mean and standard deviation computed from clutter data of the local background, $T_{G\Gamma D}$ denotes adaptive threshold respectively.

Chapter 5

Simulation Results

Dataset Description

Estimation Results

Target Detection Results

Performance Analysis

Chapter 5

Simulation Results

5.1 Dataset Description

The SAR data used for analysis has been obtained by Sandia National Laboratory with moving and stationary acquisition and recognition (MSTAR) platform [21]. The MSTAR program is joint Defense Advanced Research Projects Agency (DARPA) and Air Force Research Laboratory (AFRL) effort for development and evaluation of an advanced automatic target detection and recognition system. The files in the MSTAR dataset contain a header followed by moduli and phases of the data. The header file consists information regarding radar characteristics such as resolution, frequency, squint etc. The main features of this MSTAR system are given below in Table 5.1.

The clutter modeling was done by analyzing the SAR clutter data statistics from MSTAR images. The MSTAR target image which is analyzed possesses a single military target that is embedded within a vegetation clutter region. Experiments are conducted on HB04066.003 data file as shown in Fig. 5.1(a). This data file contains BTR-60 military target (at a depression angle of 17°) embedded within vegetation clutter. A pure clutter region in this image was selected and analyzed statistically in following subsection.

Table 5.1: Main characteristics of MSTAR system

Collectors of data	Sandia National Lab
Radar Platform Name	MSTAR
Sensor Name	Twin Otter
Range Resolution	0.3047 m
Cross Range Resolution	0.3047 m
Range Pixel Spacing	0.2021048 m
Cross Range Pixel Spacing	0.203125 m
Azimuth Beamwidth	8.8º
Elevation Beamwidth	6.8º
Polarization	HH
Central frequency	9.6 GHz
Number of Look	1

5.2 Estimation Results

In order to select an appropriate statistical model for background clutter, KL distance is computed using lognormal (LGN), Weibull (WBL), K, KK, $\mathcal{G}^0$, GΓ distribution. The obtained results are given in Table 5.2. Also, for visual comparison, the normalized histogram of SAR clutter amplitude data from Fig. 5.1(a) and estimated pdfs are shown in Fig. 5.1(b)-(c). It is evident from Fig. 5.1(b)-(c) that the KK pdf outmatches the lognormal, GΓD,$\mathcal{G}^0$,Weibull, K pdf. Furthermore, Table 5.2 shows that shows that KK pdf achieves best fitting compared to GΓD, $\mathcal{G}^0$,Weibull, lognormal, K pdf in terms of minimal KL distance.

Table 5.2. Values of K-L distance of lognormal, Weibull, K , G^0, GΓD, KK distribution for vegetation area in MSTAR BTR-60 target image

Distribution	**KL Distance**
Lognormal	0.4080
Weibull	0.3766
K	0.3654
G^0	0.3668
GΓD	0.3675
KK	0.3648

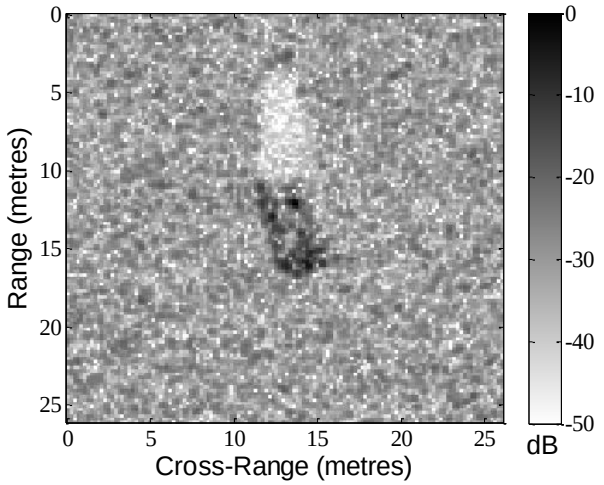

(a)

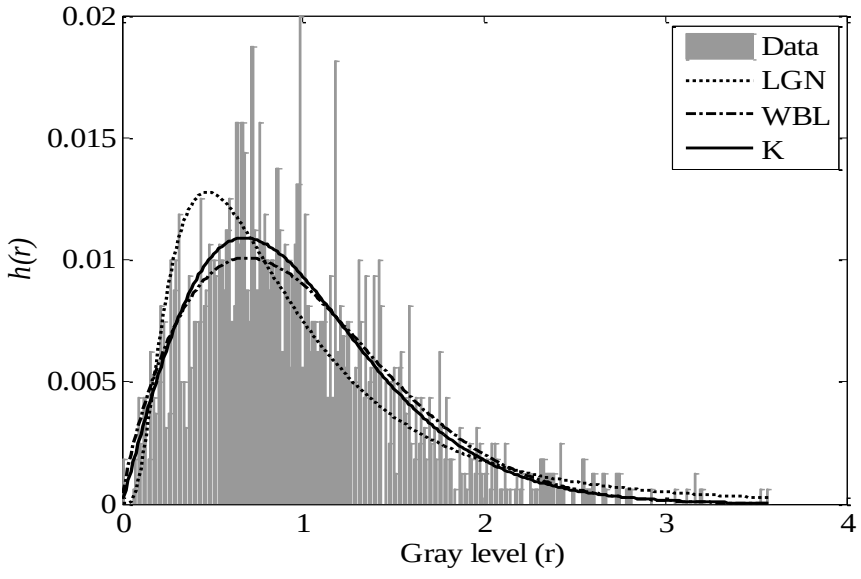

(b)

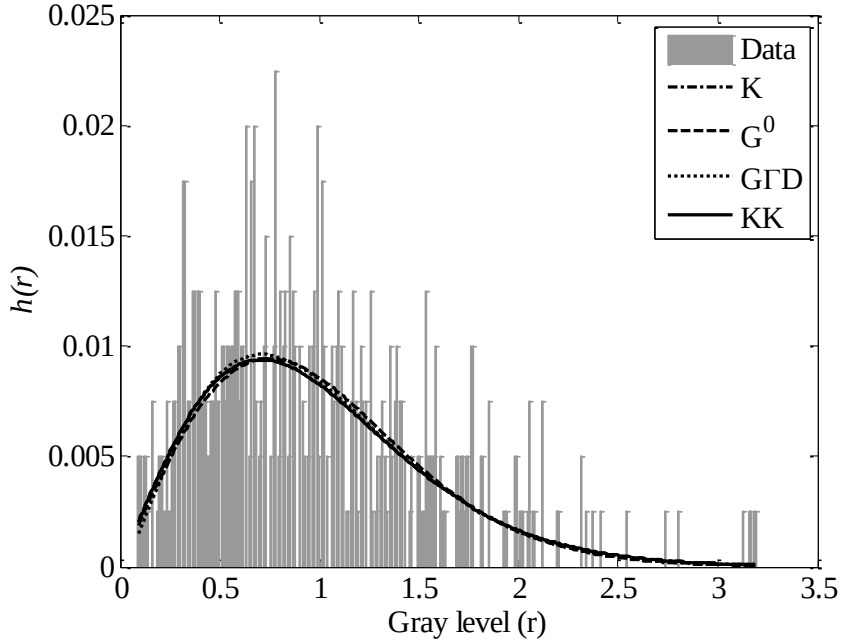

(c)

Figure. 5.1 (a) Original SAR image of BTR-60 military target with vegetation clutter (b)–(c) Estimated pdfs and data histogram of clutter region of experimental BTR-60 image

5.3 Target Detection Results

For implementation of CFAR target detection algorithm, a square shaped sliding window (CFAR stencil) of 79 × 79 pixels with a guard band of 39 × 39 pixels was used and P_{fa} was set to 0.01. The result of target detection using adaptive threshold for the lognormal distributed clutter background for image given in Fig. 5.1(a) is given in Fig. 5.2(a). Also, the detection result considering threshold for Weibull modeled clutter, threshold for K distributed clutter, threshold for G^0 modeled clutter, threshold for GΓ modeled clutter background and KK modeled clutter background are given in Fig. 5.2(b) , Fig. 5.2(c) and Fig. 5.2(d), Fig. 5.2(e) and Fig. 5.2(f). The computation time required for the test target image given in Fig. 5.1(a) is tabled in Table 5.3. The experiments are carried out using MATLAB 2010a running on Intel (R) Core(TM) i5-3317U CPU @ 1.70 GHz and 4.00-GB memory.

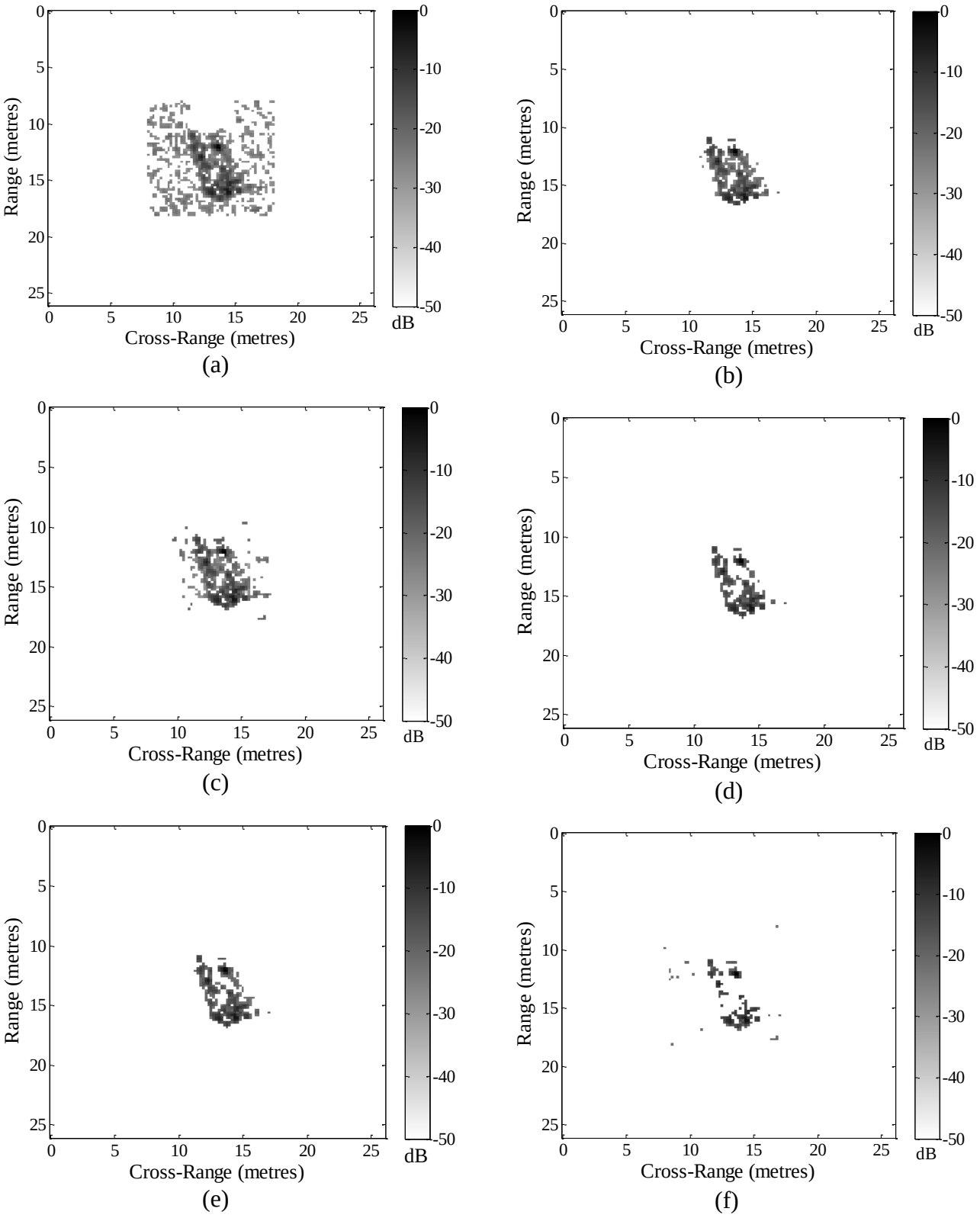

Figure. 5.2. Result of CFAR target detection algorithm for image in Fig.5.1(a) with adaptive threshold for Lognormal, Weibull, K , G^0, GΓD, KK-distributed clutter (a)-(f)

Table 5.3. Average computation time (in ms) for a single window of 79×79 for test image in Fig. 5.1(a)

Distribution	Statistics Calculation	Estimation Equations solutions	Threshold Calculation	Total Time
Lognormal	1.3454	0.0599	0.0389	1.4442
Weibull	1.4810	0.4939	0.0105	1.9854
K	2.3020	0.2495	127.1758	129.7273
G^0	0.6540	89.5396	0.0083	90.2019
GΓD	2.8945	0.0182	0.0723	2.9851
KK	2.1838	0.2378	168.3819	170.8035

5.4 Performance Analysis

The experimental analysis is provided to analyze performance of the CFAR detection algorithm. The influence from other parts should be isolated in order to validate contribution from the underlying distribution to the CFAR algorithm. A target free region from SAR image is thus chosen for such a performance analysis. The procedure for finding FAR known as CFAR maintaining performance is given as follows:

1) Background clutter: A target free region from SAR image with pure vegetation clutter is chosen. It is divided into a number of sub-images with the size of $N_1 \times N_2$ pixels, each sub-image is considered as background clutter provided by Step I of the CFAR detection algorithm in Fig. 3.1.

2) Target detection algorithm: The CFAR algorithms based on GΓD, Weibull, K, KK, G^0 and lognormal distribution are applied on each sub-image for a given P_{fa}. The pixels in each of the sub-image are compared with the respective global threshold derived from CFAR detection algorithm, and those pixels which are greater than the thresholds are considered as targets while rest pixels are treated as clutter.

3) Actual FAR computation: The mean false alarm rate (FAR) of the k^{th} sub-image is calculated for each CFAR based distribution, which is given as $R_{fa}^{(k)}$, is $R_{fa}^{(k)} = N_T^{(k)} / (N_1 \times N_2)$, where $N_T^{(k)}$ is the number of detected targets in the respective sub-image.

4) Performance analysis: When actual FARS match given P_{fa} better , the CFAR algorithm shows a better constant false alarm rate maintaining performance.

For this analysis, a pure clutter image from Fig.5.1(a) is chosen and divided into sub-images of 7×7 pixels with a guard band of 3×3 pixels. The actual mean FARs obtained from each sub-image by applying the CFAR algorithm based on different distributions for three different given P_{fa} = 0.0100, P_{fa} = 0.0200, and P_{fa} = 0.0300 are listed in Table 5.4.

Table 5.4. Mean Actual FARs corresponding Fig. 5.1(a)

Underlying Distribution	**Given** P_{fa}		
	0.01	**0.02**	**0.03**
	Mean R_{fa}		
Lognormal	0.4349	0.4391	0.4391
Weibull	0.0630	0.0777	0.0819
K	0.3046	0.3235	0.3235
G^0	0.0420	0.0399	0.0399
GΓD	0.0315	0.0462	0.0588
KK	0.1239	0.0945	0.0945

Chapter 6

Conclusion and Future Work

Conclusion

Future Work

Chapter 6

Conclusion and Future Work

6.1 Conclusion

In this study, CFAR target detection algorithm on MSTAR data was presented to detect military targets embedded within vegetation clutter. Here, Lognormal, Weibull, K, KK, G^0 and GΓD distributions are analyzed for modeling clutter amplitude of vegetation areas. The parameters of Lognormal, Weibull, G^0 and GΓD distributions are estimated by maximum likelihood estimation, moment of moments, method of log cumulants. In order to obtain parameter estimates of K distribution, the parameter estimation method higher order statistics and fractional moments is used. Semi-experiential method in KK-distribution was used for parameter estimation. Then, the adaptive threshold is computed separately for each distribution background clutter utilized for decision in detector. Experimental results are presented for comparing the adaptive CFAR detection accuracy in presence of GΓD, G^0, K, KK, Weibull and lognormal distributed clutter. The demonstrated results show that the false alarm rates for detection in GΓD and G^0 clutter are lower than the same in KK, lognormal, Weibull, K, clutter. Furthermore, computation time for execution of CFAR algorithm considering generalized Gamma distributed clutter is less than that of KK, G^0, K distribution. It can be said CFAR detector in presence of Generalized Gamma distributed clutter outmatches CFAR algorithms using lognormal, Weibull, K, KK, G^0 distributions in terms of accuracy and computation time. Therefore, it is attractive to apply the CFAR based on GΓD algorithm for the practical and real time applications.

6.2 Future Work

The target detection system can be extended to a generalized target detection system which performs well in both homogeneous and heterogeneous SAR images. The expert system oriented detection methods can also be developed by incorporating artificial intelligence systems in this target detection method.

References

[1] Xianxiang Qin, Shilin Zhou, Huanxin Zou, and Gui Gao, “A CFAR detection algorithm for generalized gamma distributed background in high-resolution SAR images,” *IEEE Geoscience and Remote Sensing Letters*, vol. 10, no. 4, pp. 806-810, 2013.

[2] M. S. Greco and F. Gini, “Statistical analysis of high-resolution SAR ground clutter data,” *IEEE Transanctions on Geoscience and Remote Sensing*, vol. 45, no. 3, pp. 566–575, 2007.

[3] S. Erfanian and V. T. Vakili, “Introducing excision switching-CFAR in K distributed sea clutter,” *Signal Processing*, vol. 89, no. 6, pp. 1023–1031, 2009.

[4] D.R. Iskander and A.M. Zoubir, “Estimation of the parameters of the K-distribution using higher order and fractional moments,” *IEEE Transanctions on Aerospace and Electronic Systems*, vol. 35, no. 4, pp. 1453-1457, 1999

[5] S. Demirci, C. Ozdemir, A. Akdagli, and E. Yigit, “Clutter reduction in synthetic aperture radar images with statistical modeling: An application to MSTAR data,” *Microwave and Optical Technology Letters*, vol. 50, no. 6, pp. 1514–1520, 2008.

[6] J.-M. Nicolas, “Introduction to second kind statistics: Application of log-moments and log-cumulants to the analysis of radar image distributions,” *Traitement du Signal*, vol. 19, no. 3, pp. 139–167, 2002.

[7] A. C. Frery, H. J. Muller, C. C. F. Yanasse, and S. J. S. Sant’Anna, “A model for extremely heterogeneous clutter,” *IEEE Transanctions on Geoscience and Remote Sensing*, vol. 35, no. 3, pp. 648–659, 1997.

[8] E. W. Stacy, “A generalization of the gamma distribution,” *Annals of Mathematical Statistics*, vol. 33, no. 3, pp. 1187–1192, 1962.

[9] H. C. Li, W. Hong, Y. R. Wu, and P. Z. Fan, “On the empirical statistical modeling of SAR images with generalized gamma distribution,” *IEEE Journal of Selected Topics in Signal Processing*, vol. 5, no. 3, pp. 386–397, 2011.

[10] M. Dohler and M. Arndt, "Inverse incomplete gamma function and its application," *Electronics Letters*, vol. 42, no. 1, pp. 46–47, 2006.

[11] Y. Gao, R. Zhan, J. Wan, J. Hu, and J. Zhang, "CFAR target detection in ground SAR image based on kk distribution," *Progress in Electromagnetics Research*, vol. 139, pp. 721-742, 2013.

[12] Y. Dong and B. Haywood, "High grazing angle X-band sea clutter distributions," *Proceedings in IET International Conference on Radar Systems*, pp. 1–5, 2007.

[13] S. Sayama and S. Ishii, "Suppression of Log-Normal Distributed Weather Clutter Observed by an S-Band Radar," *Wireless Engineering and Technology*, vol. 4, no. 3, pp. 125-133, 2013.

[14] Caner Ozdemir. Inverse synthetic aperture radar imaging with MATLAB algorithms, vol. 210. John Wiley & Sons, 2012.

[15] V Anastassopoulous and G.A.Lampropoulous, "Optimal CFAR detection in Weibull clutter," *IEEE Transaction on Aerospace and Electronic Systems*, vol. 31, no. 1, pp. 52-64, Jan 1995.

[16] J. Cheng, G. Gao, W. Ding, X. Ku, and J. Sun, "An improved scheme for parameter estimation of g° distribution model in high-resolution SAR images," *Progress in Electromagnetics Research*, vol. 134, pp. 23-46, 2013.

[17] Stacy, E. Webb, and G. Arthur Mihram, "Parameter estimation for a generalized gamma distribution," *Technometrics* vol. 7, no. 3, pp. 349-358, 1965.

[18] Khalid El-Darymli, Peter McGuire, Desmond Power, and Cecilia Monoley, "Target detection in synthetic aperture radar imagery: a state-of-the-art survey," *Journal of Applied Remote Sensing*, vol. 7, no.1, pp. 071598-071598, 2013.

[19] G.Gao, "Statistical Modeling of SAR Images: A survey," *Sensors*, vol. 10, pp. 775-795, 2010.

[20] Robert J Marks. *Handbook of Fourier analysis & its applications*, volume 800. Oxford University Press London, 2009.

[21] [Online]. Available: https://www.sdms.afrl.af.mil/index.php?collection=mstar

Publication

Dheeren Kumar Mahapatra, Kumari Rosy Pradhan, and Lakshi Prosad Roy, “An Experiment on MSTAR Data for CFAR Detection in Lognormal and Weibull Distributed SAR Clutter,” in *Proc. IEEE ICMOCE*, IIT Bhubaneswar, India, 18-20 Dec, 2015.